Journal of Ceramic Processing Research. Vol. 17, No. 8, pp. 876~880 (2016)

J O U R N A L O F
Ceramic Processing Research

Mechanochemical synthesis and rapid sintering of nanocrystalline $AlCr_2$-$2Al_2O_3$ composite and its mechanical properties

Jin-Kook Yoon[a] and In-Jin Shon[b,*]

[a]*Materials Architecturing Research Center, Korea Institute of Science and Technology, PO Box 131, Cheongryang, Seoul 130-650, Korea*
[b]*Division of Advanced Materials Engineering, the Research Center of Hydrogen Fuel Cell, Chonbuk National University, 664-14 Deokjin-dong l-ga, Deokjin-gu, Jeonju, Jeonbuk 56-756, Korea*

Nanopowders of $AlCr_2$ and Al_2O_3 were synthesized during high energy ball milling. Densely nanostructured $AlCr_2$-$2Al_2O_3$ composite was consolidated by high-frequency induction heated sintering within 2 min from milled powders. Highly dense $AlCr_2$-$2Al_2O_3$ composite with relative density of up to 96% was produced under application of a 80 MPa pressure and the induced current. The fracture toughness of a $AlCr_2$-Al_2O_3 composite in this study is similar to that of previous study, while the hardness of a $AlCr_2$-Al_2O_3 composite in this study is better than that of previous study due to the grain refinement. The fracture toughness of $AlCr_2$-$2Al_2O_3$ composite is higher than that of pure Al_2O_3. The microstructure and mechanical properties were investigated using FE-SEM with EDS and Vickers hardness tester.

Ke ywords: Sintering, Hardness, Nanocrystalline, Fracture toughness, Synthesis.

Introduction

Intermetallic compounds have long been considered to be ideal materials destined for high temperature application in the aircraft and shuttle turbine industries. Particular attention has been paid to the aluminides, especially $AlCr_2$, due to its high melting temperature, low density, excellent resistance to corrosion and oxidation. However, like many intermetallics, use of $AlCr_2$ in industry has been limited due to low fracture toughness, around 9.4 $MPa \cdot m^{1/2}$, and a low hardness of about 6.3 GPa [1]. The mechanical properties can be improved significantly by reinforcing $AlCr_2$ with hard ceramic particles such as Al_2O_3 and by fabrication of nanostructured composite [2]. Furthermore, oxidation resistance of $AlCr_2$ increased with addition of Al_2O_3 which has a density of 3.98 g/cm^3, a Young's modulus of 380 GPa, excellent oxidation resistance and good high-temperature mechanical properties [3, 4]. Hence, a microstructure consisting of $AlCr_2$ and Al_2O_3 may have sufficient oxidation resistance and high temperature mechanical properties to be a successful high temperature structural material.

Nanomaterials have received a good deal of attention recently as they possess high strength, high hardness, excellent ductility and toughness [5, 6]. In recent days, nanocrystalline powders have been developed by the thermochemical and thermomechanical process named as the spray conversion process (SCP), co-precipitation and high energy ball milling [7-9]. High energy ball milling among the methods, the raw powders can be synthesized during the milling [10, 11] and the sintering temperature of high energy mechanically milled powder is lower than that of unmilled powder due to the increased reactivity, internal and surface energies, and surface area of the milled powder, which contribute to its so-called mechanical activation [12-14]. However, the grain size in sintered materials becomes much larger than that in pre-sintered powders due to a rapid grain growth during a conventional sintering process. Therefore, even though the initial particle size is less than 100 nm, the grain size increases rapidly up to 2 μm or larger during conventional sintering [15]. So, controlling grain growth during sintering is one of the keys to the commercial success of nanostructured materials. In this regard, the high-frequency induction heated sintering method which can make dense materials within 2 min, has been shown to be effective in achieving this goal [16-18].

The purpose of this work is to synthesize nanopowders and produce dense nanocrystalline $AlCr_2$-$2Al_2O_3$ composite within 2 min using this high-frequency induction heated sintering method and to evaluate its mechanical properties (hardness and fracture toughness) and microstructure.

Experimental Procedures

Pure CrO_3 (99.99%, -325 mesh, Junsei Inc.) and pure Al (99.5%, -325 mesh, Alfa Aesar Inc.) powders were used as raw materials. $2CrO_3$ and 5Al powders were mixed in a high energy ball mill. A Pulverisette-5 planetary mill was used at 250 rpm for 20 hrs.

*Corresponding author:
Tel : +82-63-270-2381
Fax: +82-63-270-2386
E-mail: ijshon@chonbuk.ac.kr

Tungsten carbide balls (10 mm in diameter) were used for milling in a sealed cylindrical stainless steel vial under argon atmosphere. The weight ratio of ball-to-powder was 20:1.

The grain sizes were calculated by Suryanarayana and Norton's formula [19]:

$$B_r(B_{crystalline} + B_{strain})\cos\theta = k\lambda / L + \eta\sin\theta \quad (1)$$

where B_r is the full width at half-maximum (FWHM) of the diffraction peak after instrumental correction, $B_{crystalline}$ and B_{strain} are FWHM caused by the small grain size and internal stress, respectively; k is a constant (with a value of 0.9); λ is the wavelength of the X-ray radiation; L and η are the grain size and internal strain, respectively; and θ is the Bragg angle. The parameters B and B_r follow Cauchy's form with the relationship: $B = B_r + B_s$, where B and B_s are the FWHM of the broadened Bragg peak and the standard sample's Bragg peaks, respectively.

The milled powders were placed in a graphite die (outside diameter, 45 mm; inside diameter, 20 mm; height, 40 mm) and then introduced into the high-frequency induction heated sintering (HFIHS) system made by Eltek Co. in the Republic of Korea. A schematic diagram of this system is shown in Fig. 1. The HFIHS apparatus includes a 15 kW power supply and a uniaxial press with a maximum load of 50 kN. The system was first evacuated and a uniaxial pressure of 80 MPa was applied. An induced current was then activated and maintained until the densification rate became negligible, as indicated by the observed shrinkage of the sample. Sample shrinkage was measured in real time by a linear gauge measuring the vertical displacement.

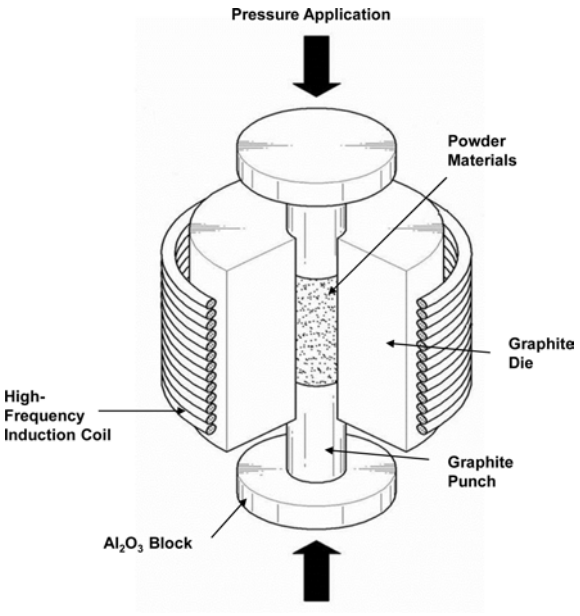

Fig. 1. Schematic diagram of the apparatus for high-frequency induction heated sintering.

Temperature was measured by a pyrometer focused on the surface of the graphite die. A temperature gradient from the surface to the center of the sample is dependent on the heating rate, the electrical and thermal conductivities of the compact, and its relative density. The heating rates were approximately 1000 K minute^{-1} during the process. At the end of the process, the current was turned off and the sample was allowed to cool to room temperature. The entire process of densification using the HFIHS technique consists of four major control stages: chamber evacuation, pressure application, power application, and cooling off. The process was carried out under a vacuum of 12 Pa.

The relative densities of the synthesized sample were measured by the Archimedes method. Microstructural information was obtained from product samples that were polished at room temperature. Compositional and micro structural analyses of the products were completed through X-ray diffraction (XRD) and scanning electron microscopy (SEM) with energy dispersive X-ray analysis (EDAX). Vickers hardness was measured by performing indentations at a load of 20 kg_f and a dwell time of 15 s on the sintered samples.

Results and Discussion

Fig. 2 indicates X-ray diffraction patterns of powders milled using high energy ball. $AlCr_2$ and Al_2O_3 peaks were identified after milling. This indicates that reaction (1) occurs during the high energy ball milling method. The interaction between $2CrO_3$ and 5Al is thermodynamically feasible;,

$$2CrO_3 + 5Al \rightarrow AlCr_2 + 2Al_2O_3 \quad (2)$$

The full width at half-maximum (FWHM) of the diffraction peak in Fig. 2 is broad due to the refinement of powders and strains. The average grain sizes of $AlCr_2$ and Al_2O_3 measured by Suryanarayana and Grant Norton's formula [19] were about 25 nm and 52 nm, respectively. Fig. 3 shows FE-SEM image and EDS analysis of $AlCr_2$ and Al_2O_3 powders synthesized

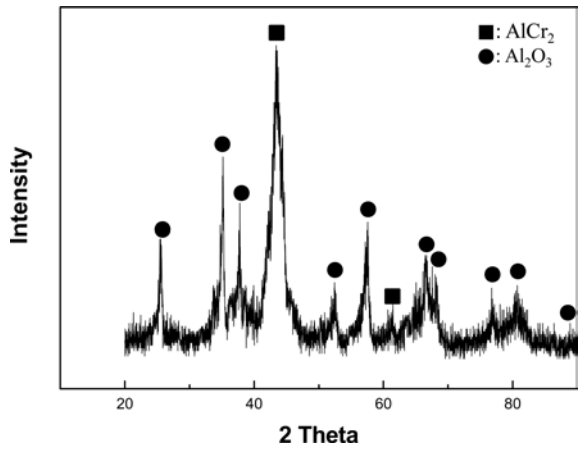

Fig. 2. XRD patterns of mechanically milled powders.

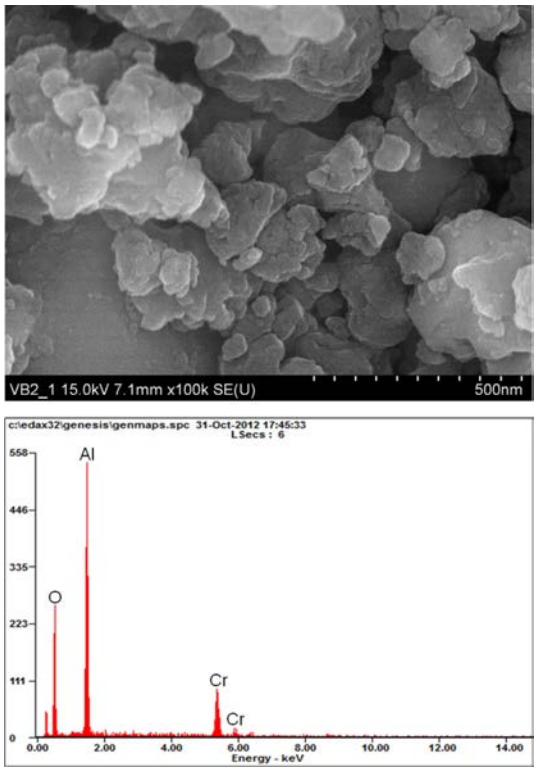

Fig. 3. FE-SEM image and EDS analysis of the $AlCr_2$ and Al_2O_3 powders milled for 20 hrs.

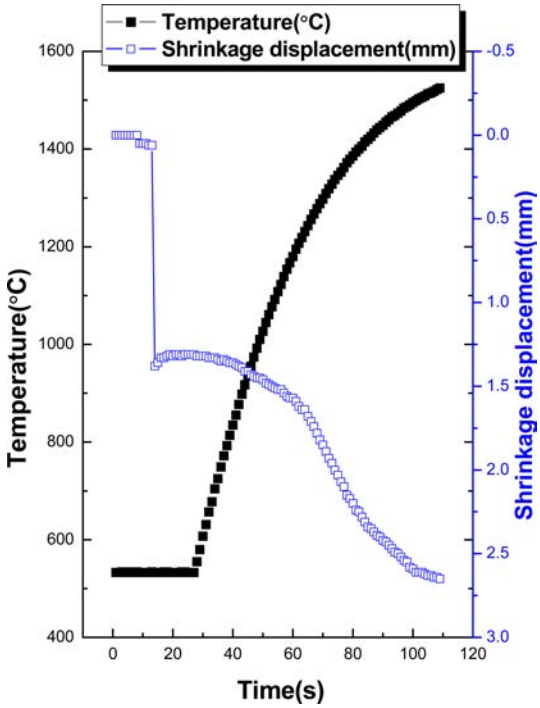

Fig. 4. Variations of temperature and shrinkage displacement with heating time during the high-frequency induction heated sintering of $AlCr_2$ and Al_2O_3 powders.

by high energy ball milling method for 20 hrs. The powders have nanocrystalline and some agglomeration. The milling process is known to introduce impurities (W and Fe) from the ball and/or container. However, in this study, peaks other than Al, Cr and O were not identified.

The variations in shrinkage displacement and temperature of the surface of the graphite die with heating time during the processing of $AlCr_2$ and Al_2O_3 powders are shown in Fig. 4. The application of the induced current resulted in shrinkage due to consolidation. As the induced current was applied, the shrinkage displacement is nearly constant up to heating time of 12 s but then abruptly increased. And the shrinkage displacement gradually increased with

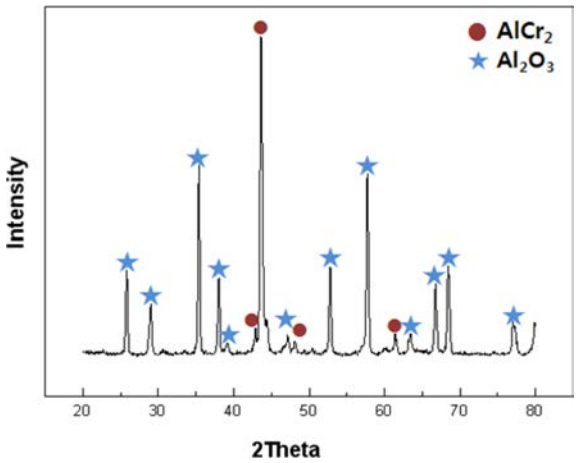

Fig. 5. XRD pattern of the $AlCr_2$-$2Al_2O_3$ composite sintered by HFIHS.

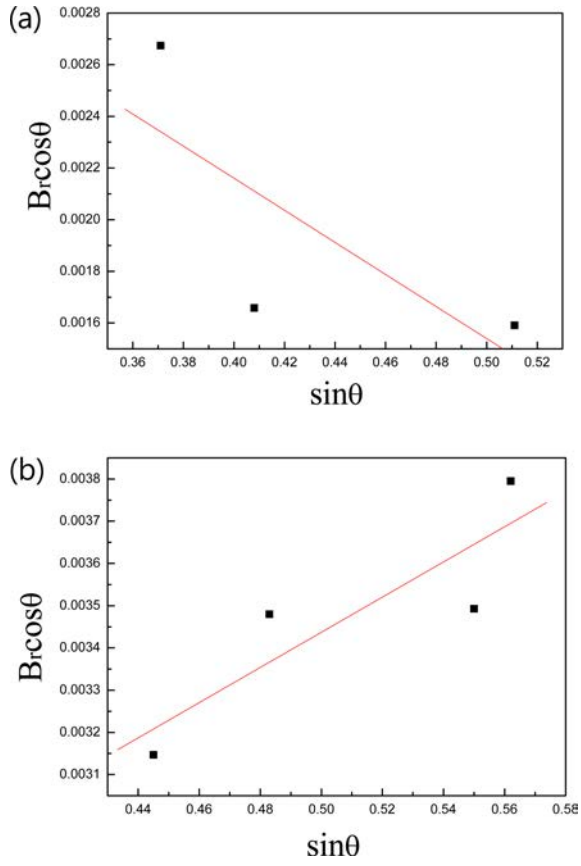

Fig. 6. Plot of $B_r$cosè versus sinè for (a) $AlCr_2$ and (b) Al_2O_3 in composite heated to 1520 °C.

temperature up to about 1520 °C. Fig. 5 shows X-ray diffraction result of a specimen heated to 1520 °C. The figure exhibit only peaks pertaining to the $AlCr_2$ and Al_2O_3. Plot of $B_r\cos\theta$ versus $\sin\theta$ for $AlCr_2$ and Al_2O_3 in composite sintered at 1520 °C is shown in Fig. 6. The average grain sizes of $AlCr_2$ and Al_2O_3 measured by Suryanarayana and Grant Norton's formula were about 35 and 103 nm, respectively. Fig. 7 shows FE-SEM image and X-ray mapping of an etched surface of the samples heated to 1520 °C under a pressure of 80 MPa. It is apparent that the $AlCr_2$ and Al_2O_3 grains consist of nanocrystallites suggesting the absence of grain growth during sintering. This retention of the fine grain structure can be attributed to the high heating rate and the relatively short exposure to the high temperature. In FE-SEM image, bright phase is $AlCr_2$ and grey phase is Al_2O_3 according to X-ray mapping and mass contrast. The corresponding relative density is about 96%.

After milling, the milled powder was consolidated by HFIHS at 1520 °C within 2 min. These powders were sintered under the application of high pressure (80MPa) which had a significant effect on the total driving force [20]. The effect of pressure on the densification of TiO_2 during high-frequency induction heated sintering was investigated by Shon et al. [21]. A significant increase in the relative density was observed as the pressure increased from about 60 to 100 MPa during sintering at 800 °C. Secondly, the role of the current in sintering has been the focus of several attempts aimed at providing an explanation for the observed enhancement of sintering and the improved characteristics of the products. The role played by the current has been interpreted in various ways, the effect being explained in terms of high Joule heating at contacts of powders, the presence of plasma in pores separating powder particles [22], and the intrinsic contribution of the current to rapid mass transport [23].

Vickers hardness measurements were made on polished sections of the $AlCr_2$-$2Al_2O_3$ composite using a 20 kg_f load and a 15 s dwell time. The calculated hardness value of $AlCr_2$-$2Al_2O_3$ composite sintered at 1520 °C from high energy ball milled powders were 792 kg/mm^2. These values represent an average of five measurements. Indentations with large enough loads produced median cracks around the indentation. The lengths of these cracks permit estimation of the fracture toughness of the materials by means of the expression [24]:

$$K_{IC} = 0.023(c/a)^{-3/2} \cdot H_v \cdot a^{1/2} \quad (3)$$

where c is the trace length of the crack measured from the center of the indentation, a is one half of the average length of the two indent diagonals, and H_v is the hardness.

As in the case of hardness values, the toughness values were derived from the average of five measurements. The toughness value of composite obtained from high energy ball milled powders are 9.5 $MPa \cdot m^{1/2}$.

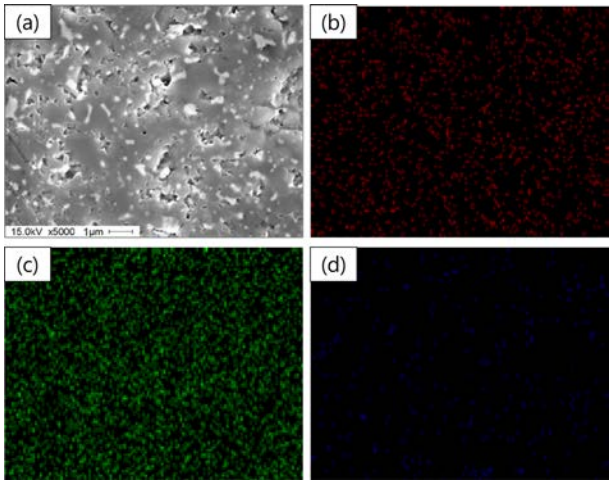

Fig. 7. FE-SEM image and X-ray mappinsg of the $AlCr_2$-$2Al_2O_3$ composite sintered by HFIHS: (a) FE-SEM image, (b) oxygen, (c) aluminum and (d) chromium.

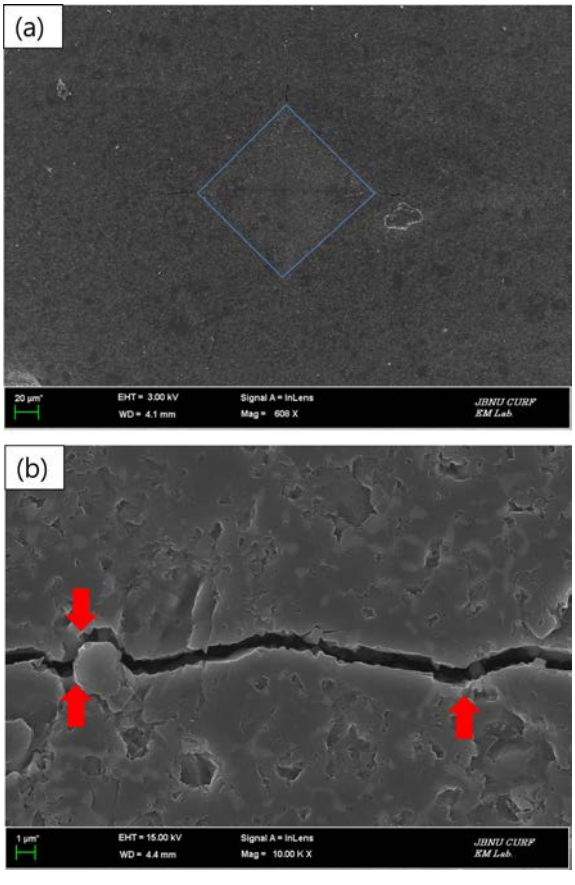

Fig. 8. (a) Vickers hardness indentation and (b) crack propagation in $AlCr_2$-$2Al_2O_3$ composite sintered by HFIHS.

The hardness and fracture toughness of $AlCr_2$-Al_2O_3 composite with grain size of several μm are reported as 6.3 GPa and 9.4 $MPa \cdot m^{1/2}$ [1]. The fracture toughness of a $AlCr_2$-$2Al_2O_3$ composite in this study is similar to that of previous study, while the hardness of a $AlCr_2$-$2Al_2O_3$ composite in this study is higher than that of previous study [1] due to the grain refinement. Fig. 8

shows Vickers indentation and crack propagating in the $AlCr_2$-$2Al_2O_3$ composite sintered using HFIHS. One to three additional cracks were observed to propagate from the indentation corner, as show in Fig. 8(a) and cracks propagated in a deflective (↑) and bowing (↓) manner, as shown in Fig. 8(b). The fracture toughness of $AlCr_2$-$2Al_2O_3$ composite is higher than that of pure Al_2O_3 reported as 4 $MPa \cdot m^{1/2}$ [25]. It is believed that $AlCr_2$ and Al_2O_3 in the composite may deter the propagation of cracks and $AlCr_2$ and Al_2O_3 have nanostructure phases.

Conclusions

The nanopowders of $AlCr_2$ and Al_2O_3 were synthesized from $2CrO_3$ and 5Al powders by high energy ball milling for 20 hrs. Using the high-frequency induction heated sintering method, the densification of nanostructured $AlCr_2$-$2Al_2O_3$ composite was accomplished from mechanically synthesized powders of $AlCr_2$ and $2Al_2O_3$. Densification can be achieved within duration of 2 min. The relative density of the composite was 96 % for the applied pressure of 80 MPa and the induced current. The average grain sizes of $AlCr_2$ and Al_2O_3 were about 35 and 103 nm, respectively. The average hardness and fracture toughness values obtained were 792 kg/mm^2 and 9.5 $MPa \cdot m^{1/2}$, respectively. The fracture toughness of a $AlCr_2$-$2Al_2O_3$ composite in this study is similar to that of previous study, while the hardness of a $AlCr_2$-$2Al_2O_3$ composite in this study is higher than that of previous study due to the grain refinement. The fracture toughness of $AlCr_2$-$2Al_2O_3$ composite is better than that of pure Al_2O_3 reported as 4 $MPa \cdot m^{1/2}$.

Acknowledgments

This work was supported by the KIST Institutional Program (Project No. 2E25374-15-096) and this work was supported by the Korea Institute of Energy Technology Evaluation and Planning (KETEP) and the Ministry of Trade, Industry & Energy (MOTIE) of the Republic of Korea (No. 20164030201070) and this research was supported by Basic Science Research Program though the National Research Foundation of Korea (NRF) funded by the Ministry of Education (2015R1D1A1A01056600).

References

1. C.L. Yeh, and J.Z. Lin, Intermetallics 33 (2013) 126-133.
2. A. Taotao, Chinese J. Aeronaut. 21 (2008) 559-564.
3. Z.W. Li, W. Gao, D.L. Zhang, and Z.H. Cai, Corrosion Science 46 (2004) 1997-2007.
4. M.F. Ashby, and D.R.H. Jones, Engineering Materials 1 (International Series on Materials Science and Technology, Vol.34), Pergamon Press, Oxford, (1986).
5. K. Niihara, and A. Nikahira, Advanced structural inorganic composite, Elsevier Scientific Publishing Co., Trieste, Italy (1990).
6. I.J. Shon, H.S. Kang, J.M. Doh, and J.K. Yoon, Met. Mater. Int. 21 (2015) 345-349.
7. Z. Fang, and J.W. Eason, Int. J. Refract. Met. Hard Mater. 13 (1995) 297-303.
8. A.I.Y. Tok, L.H. Luo, and F.Y.C. Boey, Mater. Sci. Eng. A. 383 (2004) 229-234.
9. I.J. Shon, H.G. Jo, and H.J. Kwon, Korean J. Met. Mater. 52 (2014) 343-346.
10. I.J. Shon, H.G. Jo, B.S. Kim, J.K. Yoon, and K.T. Hong, Korean J. Met. Mater. 53 (2015) 474-479.
11. S.M. Kwon, N.R. Park, J.W. Shin, S.H. Oh, B.S. Kim, and I.J. Shon, Korean J. Met. Mater. 53 (2015) 555-562.
12. B.R. Kang, J.K. Yoon, K.T. Hong, and I.J. Shon, Met. Mater. Int. 21 (2015) 698-703.
13. B.R. Kang, and I.J. Shon, Korean J. Met. Mater. 53 (2015) 320-325.
14. Bo-Ram Kang, and In-Jin Shon, Korean J. Met. Mater. 53 (2015) 225-260.
15. J. Jung, and S. Kang, Scripta Mater. 56 (2007) 561-564.
16. I.J. Shon, B.S. Kim, J.K. Yoon, K.T. Hong, and N.R. Park, Journal of Ceramic Processing Research. 16[4] (2015) 422-427.
17. H.S. Kang, and I.J. Shon, Korean J. Met. Mater. 52 (2014) 623-629.
18. I.J. Shon, Korean J. Met. Mater. 52 (2014) 573-580.
19. C. Suryanarayana, and M. Grant Norton, X-ray diffraction: a practical approach, Plenum Press, New York, (1998).
20. R.L. Coble, J. Appl. Phys. 41 (1970) 4798-4807.
21. H.C. Kim, H.K. Park, I.J. Shon, and I.Y. Ko, Journal of Ceramic Processing Research 7 (2006) 327-331.
22. Z. Shen, M. Johnsson, Z. Zhao, and M. Nygren, J. Am. Ceram. Soc. 85 (2002) 1921-1927.
23. J.E. Garay, U. Anselmi-Tamburini, Z.A. Munir, S.C. Glade, and P. Asoka-Kumar, Appl. Phys. Lett. 85 (2004) 573-575.
24. K. Niihara, R. Morena, and D.P.H. Hasselman, J. Mater. Sci. Lett. 1 (1982) 13-16.
25. M.N. Rahaman, A. Yao, B.S. Bal, J.P. Garino, and M.D. Ries, J. Am. Ceram. Soc. 90 (2007) 1965-1988.